A Journal of the Gesellschaft Deutscher Chemiker

Angewandte International Edition

GDCh

Chemie

www.angewandte.org

Accepted Article

Title: High-Index Faceted Rhodium−Antimony Nanorods for Nitrogen Fixation

Authors: Xiaoqing Huang

To be cited as: *Angew. Chem. Int. Ed.* 10.1002/anie.201915747
Angew. Chem. 10.1002/ange.201915747

Link to VoR: http://dx.doi.org/10.1002/anie.201915747
http://dx.doi.org/10.1002/ange.201915747

WILEY-VCH

10.1002/anie.201915747

WILEY-VCH

Surface Regulated Rhodium−Antimony Nanorods for Nitrogen Fixation

Nan Zhang,[1,2] Leigang Li,[1] Juan Wang,[1] Zhiwei Hu,[3] Qi Shao,[1] Xiangheng Xiao,[2] and Xiaoqing Huang*[1]

Abstract: Surface regulation has been proven to be an effective strategy to improve the performance of catalysts, but it has been rarely demonstrated for nitrogen reduction reaction (NRR) up to date. Herein, we have selectively created surface-rough Rh_2Sb nanorod (RNR) and surface-smooth Rh_2Sb NR (SNR), and investigated their performance for NRR. We found that the high-index-facet bounded Rh_2Sb RNRs/C exhibit a high NH_3 yield rate of 228.85 ± 12.96 μg h^{-1} mg^{-1}_{Rh} at -0.45 V versus reversible hydrogen electrode (RHE), outperforming the Rh_2Sb SNRs/C (63.07 ± 4.45 μg h^{-1} mg^{-1}_{Rh}) and Rh nanoparticles/C (22.82 ± 1.49 μg h^{-1} mg^{-1}_{Rh}), due to the enhanced adsorption and activation of N_2 on high-index facets. Rh_2Sb RNRs/C also show durable stability with negligible activity decay after 10 h of successive electrolysis. The present work demonstrates that surface regulation plays an important role in promoting NRR activity and provides a new strategy for creating efficient NRR electrocatalysts.

Ammonia (NH_3), the most common industrial chemical, is significant for both human beings and ecological system as a fertilizer feedstock and efficient energy carrier.[1-4] NH_3 is usually obtained by hydrogenation of nitrogen (N_2). However, the chemical inactivity, high chemical stability and low proton affinity of N_2 make it difficult for the reaction to occur. Currently, the Haber-Bosch process is still the most widely used technique for large-scale NH_3 synthesis in industry.[5] Nevertheless, it is conducted at high temperature (400-500 °C) and pressure (100-200 atm), consuming massive energy.[6, 7] In addition, most H_2 used in the Haber-Bosch process is obtained from the natural gas reforming, releasing large amounts of carbon dioxide and thereby causing serious environmental issues.[8] Therefore, it is of significance to seek a green and cost-effective method for NH_3 synthesis.

Recently, numerous efforts have been devoted to developing efficient and sustainable routes for converting N_2 to NH_3 by bio-catalysis, photocatalysis and electrocatalysis.[9-12] Particularly, electrochemical N_2 reduction reaction (NRR), powered by renewable electric energy, operates at mild conditions using water as the hydrogen source and has been attracting ever-increasing interest and efforts.[13] Despite of the progress achieved for electrochemical NRR to date, the performance of the current NRR catalysts is far from satisfactory.[14-18] The NRR performance is mainly restricted by the poor adsorption and activation of N_2 on catalysts because of the strong N≡N bond and low proton affinity of N_2.[19] Diversified strategies have been adopted to enhance the NRR performance of electrocatalysts, such as size control,[20] composition regulation,[21, 22] defect engineering,[23, 24] and ion incorporation[25]. However, surface regulation as one of the most effective strategies for catalytic performance enhancement has been rarely demonstrated for NRR up to date.

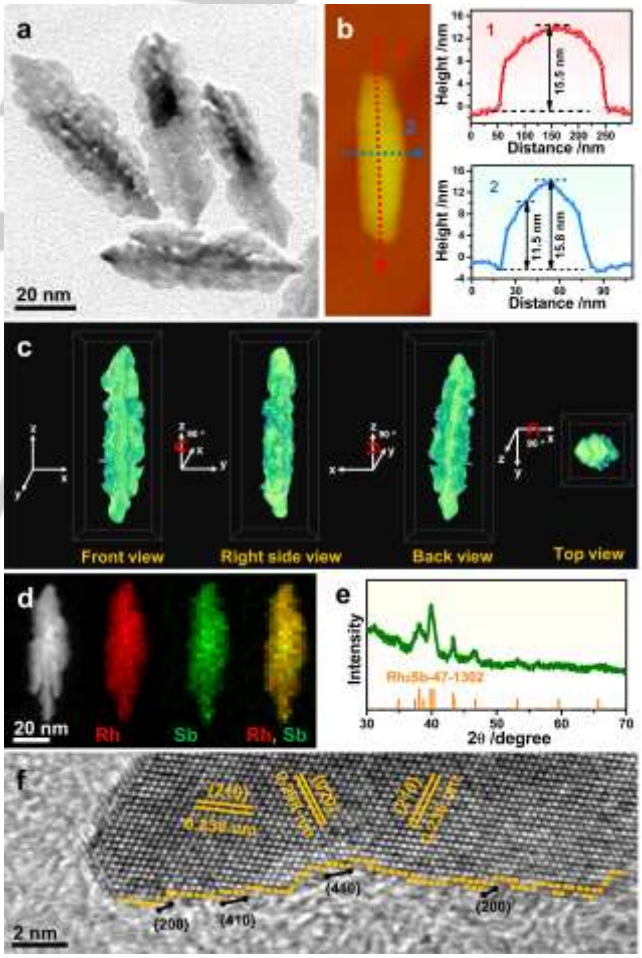

Figure 1. Morphological and structural analyses for Rh_2Sb RNRs. (a) TEM image, (b) AFM image and the corresponding height profiles of the area marked in (b), (c) four projected 3D visualization of tomographic reconstruction images, (d) HAADF-STEM image and STEM-EDS elemental mapping, (e) PXRD pattern and (f) HRTEM image of Rh_2Sb RNRs.

[1] N. Zhang, Dr. L. G. Li, J. Wang, Dr. Q. Shao, Prof. X. Q. Huang, College of Chemistry, Chemical Engineering and Materials Science Soochow University, Suzhou 215123, Jiangsu, China. E-mail: hxq006@suda.edu.cn
[2] N. Zhang, Prof. X. H. Xiao, Department of Physics and Key Laboratory of Artificial Micro- and Nano-Structures of Ministry of Education, Hubei Nuclear Solid Physics Key Laboratory, Wuhan University, Wuhan 430072, Hubei, China.
[3] Dr. Z. W. Hu, Max Planck Institute for Chemical Physics of Solids Nothnitzer Strasse 40, Dresden 01187, Germany.

Supporting information for this article is given via a link at the end of the document.

Herein, for the first time, we synthesized a class of unique surface-rough Rh_2Sb nanorods (RNRs) with high-index facets and surface-smooth Rh_2Sb nanorods (SNRs) for electrochemical NRR to demonstrate the effectiveness of surface regulation. The Rh_2Sb RNRs/C show a high NH_3 yield rate of 222.85 ± 12.96 μg h^{-1} mg^{-1}_{Rh} at -0.45 V_{RHE}, outperforming the Rh_2Sb SNRs/C (63.07 ± 4.45 μg h^{-1} mg^{-1}_{Rh}) and Rh nanoparticles (NPs)/C (22.82 ± 1.49 μg h^{-1} mg^{-1}_{Rh}) due to the ehanced adsorption and activation of N_2 on the high-index facets of Rh_2Sb RNRs/C. The Rh_2Sb RNRs/C also show durable stability with negligible activity decay after 10 h of continuous electrolysis.

The Rh_2Sb RNRs were synthesized through a facile hydrothermal process with rhodium acetate ($Rh(ac)_3$) and antimony trichloride ($SbCl_3$) as precursors, polyvinyl pyrrolidone (PVP, molecular weight = 58,000) as surfactant, N,N-Dimethylformamide (DMF) as solvent in the presence of ammonia bromide (NH_4Br). As shown by the transmission electron microscopy (TEM) images (**Figure 1a and S1**), monodisperse and uniform nanorods (NRs) with rough surface are observed. To further characterize the NRs, atomic force microscopy (AFM) was adopted to analyze the surface structure of the NRs. As displayed in **Figure 1b**, the fluctuating height profiles along both direction 1 and 2 indicate that the NR is not a planar structure. To further understand the structure of the NRs, three-dimensional (3D) tomographic reconstruction of the NRs was performed based on a series of TEM images obtained along different angles. It turns out that the NRs possess 3D structure with highly rough surfaces (**Figure 1c**). The scanning electron microscopy energy-dispersive X-ray spectroscopy (SEM-EDS) analysis shows a Rh/Sb ratio of 65.9/34.1, consistent with the feeding ratio (**Figure S2**). The elemental mapping analysis indicates uniform distribution of Rh and Sb throughout the NR (**Figure 1d**). Powder X-ray diffraction (PXRD) was employed to investigate the phase of the nanorods, where a Rh_2Sb phase was confirmed (**Figure 1e**). Based on the above analysis, it can be concluded that Rh_2Sb NRs with rough surface were synthesized and confirmed (Rh_2Sb RNRs). The high-resolution TEM (HRTEM) image of a single RNR reveals an interplanar spacing of 0.236 nm and 0.208 nm, corresponding to the {210} and {020} facet of the Rh_2Sb phase (**Figure 1f**). More interestingly, abundant steps, kinks, and high-index facets can be observed on the Rh_2Sb RNRs surface (**Figure 1f**), which may act as active sites toward enhanced catalysis.[18, 26]

To investigate the growth mechanism of the unique Rh_2Sb RNRs, the product at different reaction periods was collected and characterized by TEM, PXRD and SEM-EDS (**Figure 2 and Figure S3**). At the initial stage (45 min), substantial flocs were formed as the major product with rare NRs (**Figure 2a**). PXRD pattern indicates that the flocs are attributed to antimony oxides (Sb_2O_3) (**Figure 2g**). With the reaction proceeds (1 h), more RNRs can be observed but still with massive flocs (**Figure 2b**). Remarkably, Rh_2Sb phase appears at this stage as confirmed by PXRD (**Figure 2g**). Following this stage, more RNRs are formed with a decreased content of Sb_2O_3 (**Figure 2c, d**). Uniform RNRs were obtained with pure Rh_2Sb phase (**Figure 2e, g**). Further extension of the reaction time to 5 h did not result in obvious morphological change with preserved rod structure and Rh_2Sb phase (**Figure 2f, g**). The composition evolution was also characterized by SEM-EDS (**Figure 2h and Figure S3**). At the initial stage, the atomic ratio of Rh/Sb is close to 1:1 and then 2:1 after 2 h, consistent with the TEM and PXRD results (**Figure 2a-g**). The time-dependent composition and structure evolution reveal that the formation of Rh_2Sb RNRs involves the initial formation of Sb_2O_3, the transformation of Sb_2O_3, the reduction of Rh species, and the interdiffusion to form Rh_2Sb RNRs.

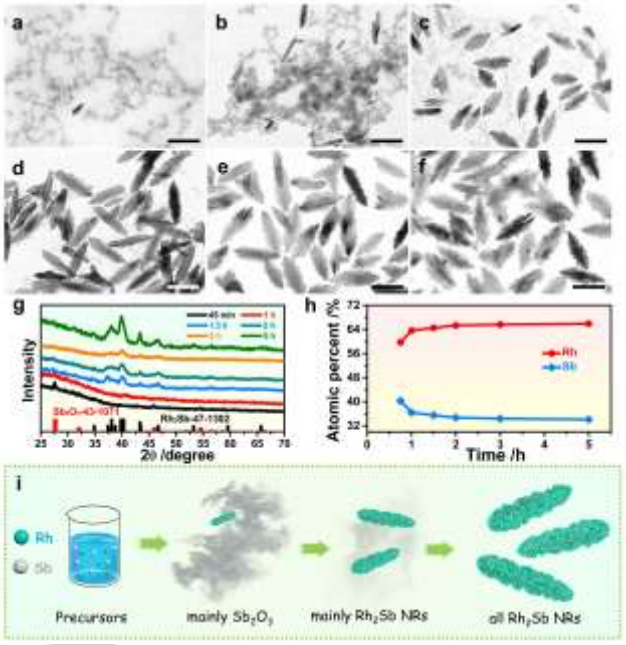

Figure 2. Growth mechanism of Rh_2Sb RNRs. (a-f) TEM images of nanocrystals produced at different reaction periods: (a) 45 min, (b) 1 h, (c) 1.5 h, (d) 2 h, (e) 3 h and (f) 5 h. (g) PXRD patterns and (h) SEM-EDS results of the intermediates produced at different reaction periods. (i) Schematic illustration of the formation of Rh_2Sb RNRs. All scale bars in (a-f) are 50 nm.

On the contrary, surface-smooth NRs (SNRs) were obtained (**Figure 3a and Figure S4**) when the amount of $SbCl_3$ in the synthesis was increased to 3.9 mg. Similar to the Rh_2Sb RNRs, the height of the SNR also fluctuates along the two scanning directions indicating a nonplanar structure (**Figure 3b**). It is worth noting that the SNRs are 3D structure but with relatively smooth surface compared with the RNRs, as confirmed by 3D visualization of tomographic reconstruction images (**Figure 3c**). The surface structure of the SNRs was further characterized by HRTEM. Based on the HRTEM image (**Figure 3d**), the surface of the NRs is smooth without obvious steps, kinks, and high-index facets (**Figure 3d**). In addition, the interplanar spacing of a single SNR is 0.226 nm, corresponding to the {211} facet of Rh_2Sb (**Figure 3d**). Besides, the SNRs demonstrate similar Rh/Sb ratio (**Figure S5**), Rh_2Sb phase (**Figure 3e**) and element distribution (**Figure 3f**) to those of Rh_2Sb RNRs.

To investigate the effect of surface structure of Rh_2Sb NRs on catalytic performance, we chose electrochemical NRR as the model reaction. Before the electrocatalytic experiments, the Rh_2Sb RNRs and Rh_2Sb SNRs were separately loaded on commercial carbon (Vulcan XC72R carbon, C) *via* sonication,

and then thoroughly washed with ethanol (**Figure S6-S7**). In addition, Rh NPs/C (**Figure S8**) was selected as a reference. Each catalyst was well dispersed in a mixture of isopropanol and Nafion by sonication and then dropped onto the electrode. The Rh mass loading was fixed at 20.0 μg for all the different catalysts as confirmed by inductively coupled plasma atomic emission spectroscopy (ICP-AES). **Figure S9** shows the CO stripping cyclic voltammograms (CVs) of all catalysts in 0.1 M $HClO_4$ solution. The electrochemical active surface area (ECSA) is 26.95 m^2 g^{-1} for Rh_2Sb RNRs/C, 19.51 m^2 g^{-1} for Rh_2Sb SNRs/C, and 44.85 m^2 g^{-1} for Rh NPs/C.

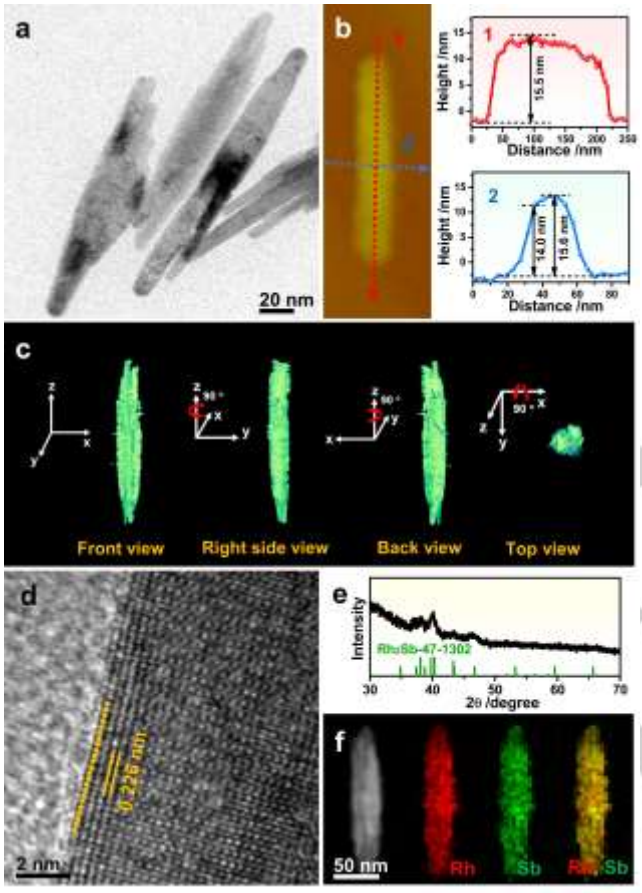

Figure 3. Morphological and structural analyses for Rh_2Sb SNRs. (a) TEM image, (b) AFM image and the corresponding height profiles of the area marked in (b), (c) four projected images of 3D visualization of tomographic reconstruction images, (d) HRTEM image, (e) PXRD pattern and (f) HAADF-STEM image and STEM-EDS elemental mapping of Rh_2Sb SNRs.

The NRR performance of the different catalysts in 0.5 M Na_2SO_4 was investigated in a H-cell separated by a proton exchanged membrane (Nafion 211) at room temperature and atmospheric pressure. Ultrahigh purity of N_2 gas (99.999%) was first purged into the cathodic chamber for at least 30 min and then bubbled with a constant flow rate of 30 sccm throughout the electrolysis process. Chrono-amperometry results of Rh_2Sb RNRs/C at -0.30 V_{RHE}, -0.35 V_{RHE}, -0.40 V_{RHE}, -0.45 V_{RHE} and -0.50 V_{RHE} were shown in **Figure 4a**. In addition, the UV-vis absorption spectra of the electrolytes stained with indophenol indicator after electrolysis for 2 h were collected to quantify the produced NH_3 by repeating for five times (**Figure S10-12**). Based on the calibration curves (**Figure S13**), the relationship between NH_3 yield rate, NH_3 Faradic efficiency (FE_{NH3}) and applied potential is shown in **Figure 4b, c.** Furthermore, the quantity, absorbance, NH_3 yield rate, and FE_{NH3}% at different potentials of the different catalysts were listed for comparison (**Table S1**). Obviously, among the three different catalysts, the Rh_2Sb RNRs/C exhibit the highest NH_3 yield rate of 228.85 ± 12.96 μg h^{-1} mg^{-1}_{Rh} and 45.77 ± 2.59 μg h^{-1} mg^{-1}_{cat} at -0.45 V_{RHE} (**Figure 4b and Table S1**), which is superior to most catalysts (**Table S2**). Furthermore, the Rh_2Sb SNRs/C and Rh NPs/C exhibit relatively low NH_3 yield rate at -0.45 V_{RHE} (**Figure 4b and Table S1**), where Rh_2Sb SNRs/C and Rh NPs/C exhibit NH_3 yield rates of 63.07 ± 4.45 μg h^{-1} mg^{-1}_{Rh} and 12.61 ± 0.89 μg h^{-1} mg^{-1}_{cat}, 22.82 ± 1.49 μg h^{-1} mg^{-1}_{Rh} and 4.56 ± 0.29 μg h^{-1} mg^{-1}_{cat}, respectively. The FE_{NH3} of Rh_2Sb RNRs/C was also superior to those of Rh_2Sb SNRs/C and Rh NPs/C (**Figure 4c and Table S1**).

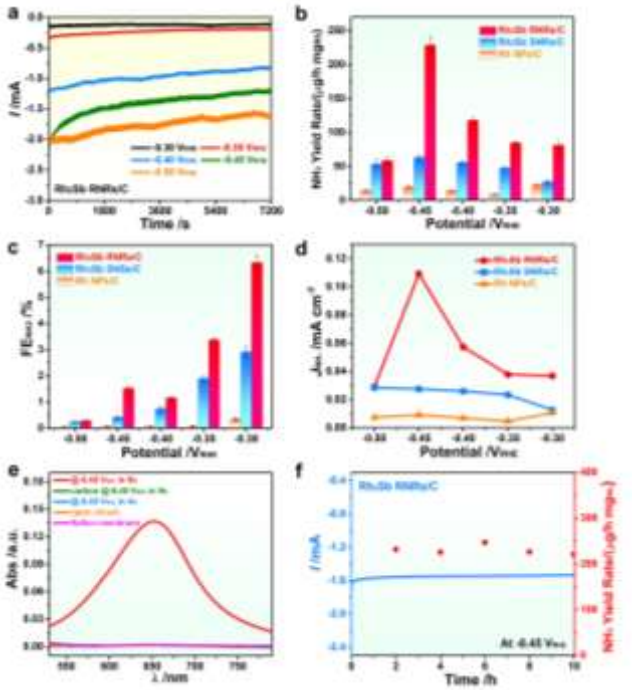

Figure 4. (a) Chrono-amperometry results of Rh_2Sb RNRs/C at different potentials. (b) Potential-dependent NH_3 yield rates, (c) FEs and (d) partial current densities of NRR at different applied potentials of Rh_2Sb RNRs/C, Rh_2Sb SNRs/C and Rh NPs/C at various applied potentials. (e) UV-vis absorption spectra of the electrolyte after electrolysis at -0.45 V_{RHE} for 2 h in Ar-saturated electrolyte (Ar gas), without Rh_2Sb RNRs (carbon), at open circuit and the electrolyte immersed in Nafion membrane, respectively. (f) Time-dependent current curve (left axis) and NH_3 yield rates (right axis) of Rh_2Sb RNRs/C at -0.45 V_{RHE}.

The ^1H nuclear magnetic resonance (NMR) spectra of the standard and the yielded $^{15}NH_4^+$ by Rh_2Sb RNRs/C at -0.45 V_{RHE}

are shown in **Figure S14a, b**. The chemical shift for isotopy-labelled sample matches well with that of standard $^{15}NH_4^+$, confirming that the yielded NH_3 was generated by electrochemical NRR over Rh_2Sb RNRs/C (**Figure S14b**). Of significant note, the amount of NH_3 produced on Rh_2Sb RNRs/C is 230.37 μg h^{-1} mg^{-1}_{Rh} as quantified by ^1H NMR result of $^{15}NH_4^+$ (**Figure S14c**). The value is very close to the corresponding value measured with indophenol blue method (228.85 ± 12.96 μg h^{-1} mg^{-1}_{Rh}). Strikingly, at various applied potentials, Rh_2Sb RNRs/C exhibit higher partial current densities of NH_3 yield than those of Rh_2Sb SNRs/C and Rh NPs/C, further confirming that the steps, kinks and high-index facets of Rh_2Sb RNRs/C may enhance the catalytic properties of NRR (**Figure 4d**). Furthermore, no hydrazine (N_2H_4) has been detected for NRR on Rh_2Sb RNRs/C (**Figure S15-S16**), indicating the high selectivity for NRR toward NH_3. To further confirm that the detected NH_3 was generated by Rh_2Sb RNRs/C during NRR, several control experiments were performed, including carbon in N_2-saturated solution at -0.45 V_{RHE}, Rh_2Sb RNRs/C in Ar-saturated solution at -0.45 V_{RHE}, Rh_2Sb RNRs/C in N_2-saturated solution at an open circuit, as well as the influence of Nafion membrane. The corresponding UV-vis spectra for all control experiments show weak signals compared to that of Rh_2Sb RNRs/C in N_2-saturated solution at -0.45 V_{RHE} (**Figure 4e and S17a**). These UV-vis experiments were repeated for three times to confirm these results (**Figure S17b-e**). The ^1H NMR spectra of these control experiments further confirm the very weak NH_3 background (**Figure S17f**). We have also demonstrated that no significant NO_2^- was detected in NaOH solution which was used to absorb NO_x in N_2, excluding the existence of NO_x (**Figure S18**). In addition, the possible existence of NO_x in N_2 was excluded by the control experiments in absence of catalysts, without applying potential, or analyzing the electrolyte after N_2 electrolysis by Rh_2Sb RNRs/C at -0.45 V_{RHE} (**Figure S19-S20**). The isotope-labelling and control experiments indicate that Rh_2Sb RNRs/C serves as an active catalyst for catalyzing the N_2 electroreduction. Furthermore, Rh_2Sb RNRs/C can keep the performance almost unchanged for 10 h (**Figure 4f**), with the morphology and chemical composition largely maintained (**Figure S21-S22**).

Considering the superior catalytic performance of Rh_2Sb RNRs/C, X-ray absorption fine structure (XAFS) spectroscopy analysis was performed to investigate the local structure of the Rh_2Sb RNRs/C at atomic scale. X-ray absorption near-edge structure (XANES) analysis shows that the Rh absorption energy for either Rh_2Sb RNRs/C or Rh_2Sb SNRs/C is between those of Rh powder and Rh_2O_3 powder (**Figure 5a**), indicating the coexistence of metal state and oxidation state. In addition, the Rh absorption energy for both catalysts are closer to that for Rh_2O_3 powder, indicating that oxidized Rh is dominant. In addition, the Rh absorption energy for Rh_2Sb RNRs/C is slightly higher than that for Rh_2Sb SNRs/C, indicating that the valence state for Rh in Rh_2Sb RNRs/C is lower than that in Rh_2Sb SNRs/C, which is consistent with the results of X-ray photoelectron spectroscopy (XPS) (**Figure S23**). The extended XAFS (EXAFS) spectra of Rh K-edge for Rh_2Sb RNRs/C and Rh_2Sb SNRs/C (**Figure 5b**) are nearly the same, indicating similar coordination environment of Rh and the strong peak at 2.36 Å is attributed to Rh-Sb metal coordination. Furthermore, the white line intensity of Rh_2Sb RNRs/C and Rh_2Sb SNRs/C is much lower than that of Rh powder and Rh_2O_3 powder, indicating a smaller coordination number of Rh for both Rh_2Sb RNRs/C and Rh_2Sb SNRs/C. Importantly, compared with the Rh_2Sb SNRs/C, the white line intensity of Rh_2Sb RNRs/C is even lower, showing a much smaller coordination number of Rh in Rh_2Sb RNRs/C. This result has reinforced the presence of high-index facets on the surface of Rh_2Sb RNRs/C, which is consistent with the HRTEM observation. Rh with unsaturated coordination would be more conducive to small molecule activation.

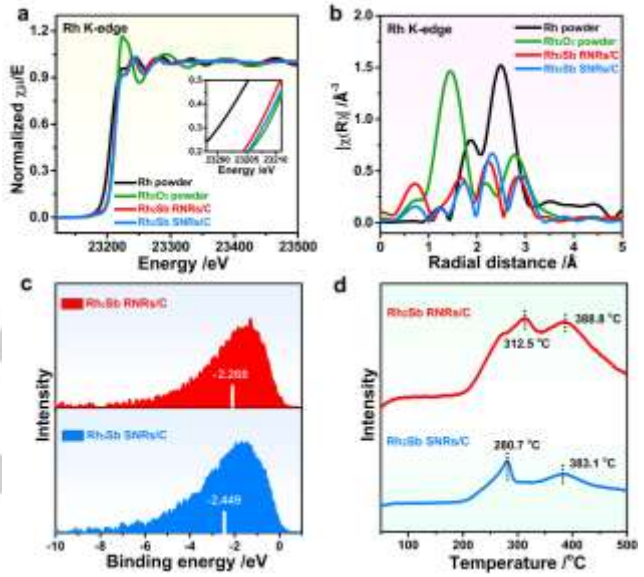

Figure 5. (a) XANES spectra and (b) EXAFS spectra of Rh K-edge of Rh powder, Rh_2O_3 powder, Rh_2Sb RNRs/C and Rh_2Sb SNRs/C. (c) Surface valence band photoemission spectra, and (d) N_2-TPD profiles for the Rh_2Sb RNRs/C and Rh_2Sb SNRs/C.

Furthermore, the binding strength between intermediates and catalysts greatly affects the catalytic performance. To evaluate the binding behavior of adsorbates on Rh_2Sb RNRs/C (-2.268 eV) and Rh_2Sb SNRs/C (-2.449 eV), the d-band center refered to $E-E_F$ is obtained. **Figure 5c** shows the d-band center of Rh_2Sb RNRs/C shifts upwards compared to that of Rh_2Sb SNRs/C, thereby likely strengthening the adsorption of N_2 and intermediates. For NRR, Rh_2Sb RNRs/C could adsorb and activate N_2 more easily, generating the enhanced performance.[27] To further evaluate the adsorption of N_2 molecules, N_2 temperature-programmed desorption (N_2-TPD, **Figure 5d**) was measured. The chemical desorption temperatures for Rh_2Sb RNRs/C (312.5 °C and 388.8 °C) are higher than those of Rh_2Sb SNRs/C (280.7 °C and 383.1 °C), which is consistent with N_2 adsorption capacity. The enhanced peak intensity of Rh_2Sb RNRs/C at higher temperature suggests that the surface high-index facets may promote the chemisorption ability and capability of N_2.[28, 29] Above all, the strong adsorption and activation of N_2 contribute to the enhanced performance of Rh_2Sb RNRs/C during NRR.

To summarize, we have successfully created a new class of Rh_2Sb RNRs with high-index facets for NRR for the first time. Time-dependent study reveals that the formation of Rh_2Sb RNRs mainly involves the initial formation of Sb_2O_3, the transformation of Sb_2O_3, the reduction of Rh species, and the interdiffusion to form Rh_2Sb RNRs. The Rh_2Sb RNRs/C exhibit a high NH_3 yield rate of 228.85 ± 12.96 μg h^{-1} mg^{-1}_{Rh} at -0.45 V_{RHE} in 0.5 M Na_2SO_4, outperforming Rh_2Sb SNRs/C and Rh NPs/C, due to the enhanced adsorption and activation of N_2 on high-index facets of Rh_2Sb RNRs/C. Rh_2Sb RNRs/C also show durable electrochemical stability with negligible activity decay after continuous electrolysis for 10 h. The present work demonstrates the important role of surface regulation of catalysts in boosting NRR performance and provides a new strategy for creating efficient NRR electrocatalysts.

Acknowledgements

This work was financially supported by the Ministry of Science and Technology (2016YFA0204100, 2017YFA0208200), the National Natural Science Foundation of China (21571135), Young Thousand Talented Program, Natural Science Foundation of Jiangsu Higher Education Institutions (17KJB150032), the project of scientific and technologic infrastructure of Suzhou (SZS201708), the Priority Academic Program Development of Jiangsu Higher Education Institutions (PAPD), and the start-up supports from Soochow University.

Keywords: Rh-Sb • Nanorod • Surface regulation • High-index facet • Nitrogen reduction reaction

[1] J. G. Chen, R. M. Crooks, L. C. Seefeldt, K. L. Bren, R. M. Bullock, M. Y. Darensbourg, P. L. Holland, B. Hoffman, M. J. Janik, A. K. Jones, M. G. Kanatzidis, P. King, K. M. Lancaster, S. V. Lymar, P. Pfromm, W. F. Schneider, R. R. Schrock, *Science* **2018**, *360*, eaar6611.

[2] K. A. Brown, D. F. Harris, M. B. Wilker, A. Rasmussen, N. Khadka, H. Hamby, S. Keable, G. Dukovic, J. W. Peters, L. C. Seefeldt, P. W. King, *Science* **2016**, *352*, 448-450.

[3] C. Guo, J. Ran, A. Vasileff, S. Z. Qiao, *Energy Environ. Sci.* **2018**, *11*, 45-56.

[4] S. Wang, F. Ichihara, H. Pang, H. Chen, J. Ye, *Adv. Funct. Mater.* **2018**, *28*, 1803309.

[5] M. Kitano, Y. Inoue, Y. Yamazaki, F. Hayashi, S. Kanbara, S. Matsuishi, T. Yokoyama, S. W. Kim, M. Hara, H. Hosono, *Nat. Chem.* **2012**, *4*, 934-940.

[6] C. J. M. van der Ham, M. T. M. Koper, D. G. H. Hetterscheid, *Chem. Soc. Rev.* **2014**, *43*, 5183-5191.

[7] Y. Zhao, Y. Zhao, R. Shi, B. Wang, G. I. N. Waterhouse, L. Z. Wu, C.-H. Tung, T. Zhang, *Adv. Mater.* **2019**, *31*, 1806482.

[8] M. Li, H. Huang, J. Low, C. Gao, R. Long, Y. Xiong, *Small Methods* **2019**, *3*, 1800388.

[9] Y. Luo, G. F. Chen, L. Ding, X. Chen, L. X. Ding, H. Wang, *Joule* **2019**, *3*, 279-289.

[10] M. Wang, S. Liu, T. Qian, J. Liu, J. Zhou, H. Ji, J. Xiong, J. Zhong, C. Yan, *Nat. Commun.* **2019**, *10*, 341.

[11] S. Wang, X. Hai, X. Ding, K. Chang, Y. Xiang, X. Meng, Z. Yang, H. Chen, J. Ye, *Adv. Mater.* **2017**, *29*, 1701774.

[12] N. Zhang, A. Jalil, D. Wu, S. Chen, Y. Liu, C. Gao, W. Ye, Z. Qi, H. Ju, C. Wang, X. Wu, L. Song, J. Zhu, Y. Xiong, *J. Am. Chem. Soc.* **2018**, *140*, 9434-9443.

[13] Y. C. Hao, Y. Guo, L. W. Chen, M. Shu, X. Y. Wang, T. A. Bu, W. Y. Gao, N. Zhang, X. Su, X. Feng, J. W. Zhou, B. Wang, C. W. Hu, A. X. Yin, R. Si, Y. W. Zhang, C. H. Yan, *Nat. Catal.* **2019**, *2*, 448-456.

[14] Z. Geng, Y. Liu, X. Kong, P. Li, K. Li, Z. Liu, J. Du, M. Shu, R. Si, J. Zeng, *Adv. Mater.* **2018**, *30*, 1803498.

[15] E. Skúlason, T. Bligaard, S. Gudmundsdóttir, F. Studt, J. Rossmeisl, F. Abild-Pedersen, T. Vegge, H. Jónsson, J. K. Nørskov, *Phys. Chem. Chem. Phys.* **2012**, *14*, 1235-1245.

[16] X. Liu, Y. Jiao, Y. Zheng, M. Jaroniec, S.-Z. Qiao, *J. Am. Chem. Soc.* **2019**, *141*, 9664-9672.

[17] H. Tao, C. Choi, L. X. Ding, Z. Jiang, Z. Han, M. Jia, Q. Fan, Y. Gao, H. Wang, A. W. Robertson, S. Hong, Y. Jung, S. Liu, Z. Sun, *Chem* **2019**, *5*, 204-214.

[18] H. M. Liu, S. H. Han, Y. Zhao, Y. Y. Zhu, X. L. Tian, J. H. Zeng, J. X. Jiang, B. Y. Xia, Y. Chen, *J. Mater. Chem. A* **2018**, *6*, 3211-3217.

[19] J. Deng, J. A. Iñiguez, C. Liu, *Joule* **2018**, *2*, 846-856.

[20] M. M. Shi, D. Bao, B. R. Wulan, Y. H. Li, Y. F. Zhang, J. M. Yan, Q. Jiang, *Adv. Mater.* **2017**, *29*, 1606550.

[21] M. M. Shi, D. Bao, S. J. Li, B. R. Wulan, J. M. Yan, Q. Jiang, *Adv. Energy Mater.* **2018**, *8*, 1800124.

[22] C. J. H. Jacobsen, S. Dahl, B. S. Clausen, S. Bahn, A. Logadottir, J. K. Nørskov, *J. Am. Chem. Soc.* **2001**, *123*, 8404-8405.

[23] X. Li, T. Li, Y. Ma, Q. Wei, W. Qiu, H. Guo, X. Shi, P. Zhang, A. M. Asiri, L. Chen, B. Tang, X. Sun, *Adv. Energy Mater.* **2018**, *8*, 1801357.

[24] C. Lv, Y. Qian, C. Yan, Y. Ding, Y. Liu, G. Chen, G. Yu, *Angew. Chem. Int. Ed.* **2018**, *57*, 10246-10250.

[25] G. F. Chen, X. Cao, S. Wu, X. Zeng, L. X. Ding, M. Zhu, H. Wang, *J. Am. Chem. Soc.* **2017**, *139*, 9771-9774.

[26] B. Lim, M. Jiang, P. H. C. Camargo, E. C. Cho, J. Tao, X. Lu, Y. Zhu, Y. Xia, *Science* **2009**, *324*, 1302-1305.

[27] B. Jiang, X. G. Zhang, K. Jiang, D. Y. Wu, W. B. Cai, *J. Am. Chem. Soc.* **2018**, *140*, 2880-2889.

[28] A. Zhang, R. He, H. Li, Y. Chen, T. Kong, K. Li, H. Ju, J. Zhu, W. Zhu, J. Zeng, *Angew. Chem. Int. Ed.* **2018**, *57*, 10954-10958.

[29] A. Zhang,J. Yang, Y. Guo, R. Jiang, F. Qin, H. Zhang, W. Lu, J. Wang, J. C. Yu, *J. Am. Chem. Soc.* **2018**, *140*, 8497-8508.

10.1002/anie.201915747

WILEY-VCH

Entry for the Table of Contents

COMMUNICATION

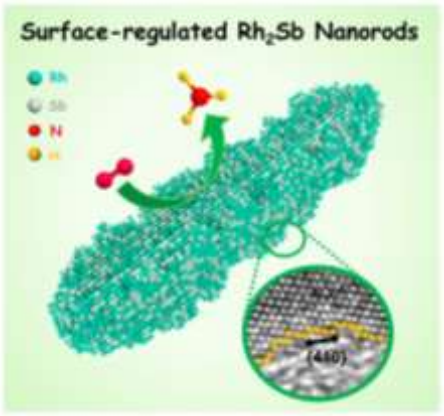

*Nan Zhang, Leigang Li, Juan Wang, Zhiwei Hu, Qi Shao, Xiangheng Xiao, and Xiaoqing Huang**

Surface Regulated Rhodium−Antimony Nanorods for Nitrogen Fixation

Rhodium-Antimony Nanorods: A unique class of surface-rough Rh_2Sb nanorobs (RNRs) was constructed for the first time. Rh_2Sb RNRs/C showed enhanced N_2 reduction reaction (NRR) performance with NH_3 yield rate of 228.85 ± 12.96 μg h^{-1} mg^{-1}_{Rh} at -0.45 V_{RHE}, outperforming the surface-smooth Rh_2Sb NRs/C, as well as the Rh nanoparticles/C, demonstrating the important role of surface regulation in boosting NRR.